



PCCP

Infrared Spectroscopy of 2-Oxo-Octanoic Acid in Multiple Phases

Journal:	<i>Physical Chemistry Chemical Physics</i>
Manuscript ID	CP-ART-11-2021-005345.R2
Article Type:	Paper
Date Submitted by the Author:	20-Feb-2022
Complete List of Authors:	Kappes, Keaten; University of Colorado Boulder, Department of Chemistry ; CIRES Frandsen, Benjamin Normann; University of Colorado Boulder, Department of Chemistry ; CIRES Vaida, Veronica; University of Colorado Boulder, Department of Chemistry ; CIRES

SCHOLARONE™
Manuscripts

ARTICLE

Infrared Spectroscopy of 2-Oxo-Octanoic Acid in Multiple Phases

Keaten Kappes^{a,b}, Benjamin N. Frandsen^{a,b} and Veronica Vaida^{a,b,*}Received 00th January 20xx,
Accepted 00th January 20xx

DOI: 10.1039/x0xx00000x

Alpha-keto acids are environmentally and biologically relevant species whose chemistry has been shown to be influenced by their local environment. Vibrational spectroscopy provides useful ways to probe the potential inter- and intramolecular interactions available to them in several phases. We measure and compare the IR spectra of 2-oxo-octanoic acid (2OOA) in the gas phase, solid phase, and at the air-water interface. With theoretical support, we assign many of the vibrational modes in each of the spectra. In the gas phase, two types of conformers are identified and distinguished, with the intramolecularly H-bonded form being the dominant type, while the second conformer type identified does not have an intramolecular hydrogen bond. The Van der Waals interactions between molecules in solid 2OOA manifest C-H and C=O vibrations lower in energy than in the gas phase and we propose an intermolecular hydrogen bonding scheme for the solid phase. At the air-water interface the hydrocarbon tails of 2OOA do interact with each other while the carbonyls appear to interact with water in the subphase, but not with neighboring 2OOA as might be expected of a closely packed surfactant film.

Introduction

In the natural environment, reactions and interactions occur under different conditions, in multiple phases, and at interfaces. Infrared (IR) spectroscopy allows investigation of molecules as they interact with their surroundings. We report on the vibrational spectroscopy of alpha-keto acids and compare the spectra in different phases significant to the natural environment. Alpha-keto acids are involved in intra- and intermolecular interactions and are therefore amenable to study by IR spectroscopy. Pyruvic acid (PA) is the smallest and best studied alpha-keto acid. The gas phase IR spectroscopy of pyruvic acid has been reported in the literature, with its vibrational modes and conformation distribution well characterized in different environments.¹⁻⁵ It has been shown that the balance between intra- and intermolecular hydrogen bonding is the dominant factor in determining PA conformation which ultimately influences its chemistry and photochemistry.^{1,6,7} Pyruvic acid spectroscopy provides a comparison for 2-oxo-octanoic acid (2OOA) with which it shares the carboxylic acid and alpha ketone functional groups, characteristic of keto acids. In addition, 2OOA has a 6-carbon alkyl chain compared with PA's single methyl group, which adds hydrophobic character to the molecule and enhances partitioning to the surface of water. The lowest energy conformers of all alpha-keto acids exhibit an intramolecular hydrogen bond between the acidic hydrogen and ketonic carbonyl in the gas phase. See Figure 1 for a visual

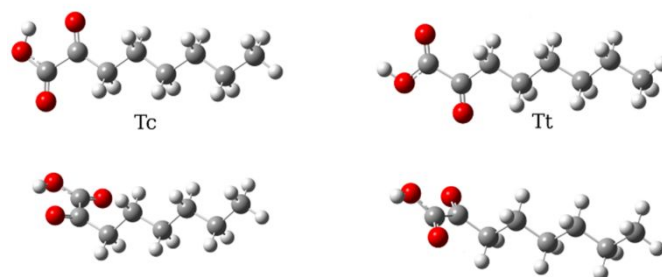


Figure 1. Conformers of 2OOA. The top row shows the alkyl tails in an all trans conformer while the bottom row includes a C2-C3 gauche orientation.

representation of select 2OOA conformers. However, the nonpolar tail of alpha-keto acids may change how the molecule interacts with its surroundings. As such, the conformations and orientations of alpha-keto acids in different environments, which ultimately determine their chemistry, may be influenced by their aliphatic chain.

In this study, we will investigate 2OOA but use what is already known about PA as an important comparison. Alpha-keto acids, and especially PA, have been at the centre of previous studies due to their presence in biology and in the natural environment.⁸⁻¹⁵ As a semi-volatile organic compound, PA is found in the atmosphere where its lifetime is determined by sunlight-initiated photolysis.^{6,16} Its photochemical products, reaction rates, and reaction mechanisms have been determined.^{3,4,16-27} The effect of water on its conformer distribution has also been experimentally and computationally investigated and its effect on PA's chemistry reported.^{1,28-33} Oxoacids are also found in oceans and aerosol particles, and their aqueous phase photochemistry has been extensively investigated.³⁴⁻⁴⁵ The main photochemical products of alpha-keto acids in aqueous solution are lipid-like oligomers that influence the formation and properties of secondary organic

^a Department of Chemistry, University of Colorado-Boulder, UCB 215, Boulder, CO 80309

^b Cooperative Institute for Research in Environmental Sciences, University of Colorado-Boulder, UCB 216, Boulder, CO 80309

*Email: Vaida@colorado.edu

Electronic Supplementary Information (ESI) available: See DOI: 10.1039/x0xx00000x

aerosols,^{15,46} which are detrimental to human health and influential on Earth's climate.^{15,47,48} In aqueous solution, there has been some commentary on the differences manifested by alpha-keto acid tail length. Specifically, Rapf *et al.*⁴⁵ demonstrated that the established photochemical mechanisms for the aqueous photochemistry of PA were generalizable to the entire class of alpha-keto acids but identified an additional Norrish Type II pathway only accessible to the larger member of the class with at least 5 total carbons.

Amphiphilic molecules like alpha-keto acids provide a critical link between the bulk ocean and the atmosphere, as they partition to the ocean surface where sea spray aerosolizes them into the atmosphere.⁴⁹⁻⁵¹ Air-water interfaces found at the sea surface microlayer and the surface of atmospheric aerosols are natural reaction environments and the surface of water has attracted increasing attention for its unique reaction conditions and ability to accelerate or even initiate chemistry not favorable in the bulk aqueous phase.^{5,49-71} Oxoacids with longer hydrophobic tails, which are expected to reside at the surface, may align or order at the water interface while the hydrophilic head group may be able to interact with interfacial water. Regardless, the asymmetric nature of the air-water interface will provide ample opportunities for intermolecular interactions and interesting chemistry.

Surface specific methods used to study the air-water interface include second-harmonic generation,⁷²⁻⁷⁴ X-ray photoelectron spectroscopy,⁷⁵ sum-frequency generation (SFG),⁷⁶⁻⁸⁹ and Infrared Reflectance Absorption Spectroscopy (IRRAS).^{56,57,90-101} Of these, IRRAS and SFG allow for vibrational characterization of molecules and also provide information about the surface morphology including orientation and packing of interfacial species. One advantage of SFG is the stringent surface selectivity inherent to these non-linear techniques which only observe anisotropic, non-centrosymmetric species in a medium without inversion symmetry, like the air-water interface.^{79,102} Though the interpretation of vibrational SFG signals is relatively complicated, as they are comprised of both resonant and nonresonant components,¹⁰² SFG has been successfully applied to study interfacial oxoacids, specifically PA. Gordon *et al.*⁸⁰ measured and assigned the surface spectrum of a PA solution and identified the hydrated diol form of PA, parapyruvic acid, and zymonic acid, at the surface, the latter two of which are oligomeric species known to spontaneously form from PA in aqueous environments. The Gordon *et al.*⁸⁰ work showcases the utility of SFG for the investigation of oxoacids and further highlights the need to understand their interfacial phenomena.

IRRAS is another surface selective technique which can provide orientation information for interfacial species while being relatively straightforward to interpret. Here we use IRRAS to obtain an IR spectrum of 2OOA at the air-water interface, where the comparison to IR spectra of this molecule in different environments may be possible and directly comparable. We also present, for the first time to our knowledge, the gas phase IR spectrum of 2OOA which provides a database for the

vibrational spectroscopy of this molecule. With theoretical support we can assign many spectroscopic features to specific vibrational modes. We record and compare gas phase IR, IRRAS, and solid Attenuated Total Reflectance (ATR) spectra of 2OOA to highlight the inter- and intra- molecular interactions in each environment, and comment on their effect on the spectra in order to glean structural, orientational, and conformational information about 2OOA in different environments. The 2OOA spectra are compared to those of PA to investigate the effect of the alkyl tail length on the properties of 2OOA at the water surface.

Experimental

Materials

2-Oxo-octanoic acid (2OOA; $\geq 99\%$) was procured from Sigma-Aldrich and used without further purification. Pyruvic acid (PA; 98%) from Sigma-Aldrich was distilled prior to use. Solutions of 6 mM 2OOA (pH = 2.57 ± 0.11) and 100 mM PA (pH = 1.8) were made with MilliQ Water (18.2 M Ω ; 3 ppb TOC) and were sonicated and filtered prior to use. Solution pH was measured with a Corning pH meter and adjusted with sodium hydroxide (98.0%, Fisher Scientific) or hydrochloric acid (37%, Mallinckrodt).

Methods

Gas Phase FTIR. The gas phase spectrum of 2OOA was obtained with the external Mid IR beam of a Bruker IFS 66 v/s FTIR spectrometer equipped with an external liquid N₂ cooled MCT detector. Solid 2OOA, which has a melting point of 33-36 °C, was placed in a glass cell with a 0.50 m path length and equipped with CaF₂ windows. For both the background and sample measurements, the cell was evacuated with an Edwards 18 rotary vane two-stage vacuum pump to a pressure of 0.112 Torr as measured by an MKS Baratron capacitance manometer (Type 626) at a temperature of 23 °C. 0.112 Torr was roughly the minimum pressure attainable by our setup and is not indicative of a 2OOA saturated vapor pressure but is mainly residual laboratory air. Solid 2OOA remained in the bottom of the cell during sample measurements. Each spectrum is the result of 200 scans at a resolution of 0.25 cm⁻¹ and the spectrum presented here is the average of 5 spectra collected consecutively for a total of 1000 scans. Plastic sheeting was used to enclose the space between the spectrometer and MCT detector which was purged with CO₂ scrubbed dry air to mitigate external CO₂ and H₂O interference in the vibrational spectra.

Attenuated Total Reflectance (ATR) IR Spectroscopy. A commercial Agilent Technologies Cary 630 FTIR ATR was used to obtain ATR IR spectra for solid 2OOA. ATR IR Spectra were recorded with an 8 cm⁻¹ resolution and a spectrum consists of 16 scans.

Infrared Reflection-Absorption Spectroscopy (IRRAS). IR spectra of 2OOA and PA at the air-water interface were

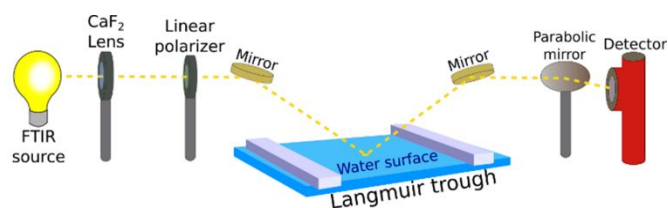


Figure 2. Schematic representation of the Infrared Reflection-Absorption Spectroscopy (IRRAS) setup.

obtained using a homebuilt IRRAS setup. A Langmuir trough held the solution of interest while an external MIR beam of a Bruker Tensor 27 was passed through a CaF_2 lens and linear polarizer before reflecting off a gold mirror at an angle of 60° relative to the surface normal, see Figure 2. After reflecting off the solution interface, another gold mirror directs the IR beam to a parabolic mirror and finally into a liquid N_2 cooled MCT detector. All external optics, the Langmuir trough, and MCT detector were enclosed in a metal box and purged with dry air before and during all scans.

The spectra presented here are Reflectance-Absorbance (RA) where $\text{RA} = -\log(R/R_0)$ and R and R_0 are the reflectivity of the keto acid containing solution and pure water, respectively. Each spectrum is comprised of 500 scans at a resolution of 1 cm^{-1} and the spectra shown here are averages of up to 6 spectra collected consecutively. The OPUS software from Bruker was used to record and compile the IRRAS spectra and the “Atmospheric Compensation” tool in OPUS was used to subtract the background from the sample spectra to mitigate interference from water vapor and CO_2 .

The 60° angle of incidence was chosen as a tradeoff to maximize absorbance of the IR light by surface species by P-polarized light while maintaining a significant interaction with S-polarized light.^{103,104} The definition of “S” and “P” polarization is not always consistent across the literature so here we define them unambiguously with the S-polarization meaning the light’s electric field is aligned parallel to the water surface and thus perpendicular to the surface normal. Thus, the definition of P-polarization is simply that it is perpendicular to the S-polarization. At angles $0^\circ < \theta < 90^\circ$, as in our experiment, the P-polarization is neither perpendicular nor parallel to the surface normal or water surface plane and thus it is best defined in its relation to the S-polarization. At the chosen angle, absorption peaks are expected to be negative for S-polarized light and positive for P-polarized light.^{96,103-106} This happens because the presence of surface species strongly affects the imaginary part of the refractive index at the interface, around the vibrational transitions in molecules, which influences reflection of light by the surface. Since our absorbance signals are much more intense in the S-polarization than the P-polarization, we exclusively use data from the S-polarized spectra to make assignments while the P-polarized data were only used to support the assignments made in the S-polarized spectra. For additional details about IRRAS we refer the interested reader to the literature.¹⁰⁶⁻¹¹¹

Computational methods. Computational chemistry was employed to aid assignments in the experimental spectra and suggest which 2OOA conformers could be observed experimentally. The computational chemistry results reported in this work were obtained using the Gaussian 16 program for DFT calculations.¹¹² Initially, a thorough conformer search was carried out. The MSTor program was used to conveniently perform a systematic conformer search by rotating along all flexible dihedral angles and generate input files.^{113,114} In 2OOA this involves rotating 120 degrees along the C-C bonds involving sp^3 hybridized carbon atoms (3-fold rotation), excluding the terminal $\text{CH}_3\text{-CH}_2$ bond due to redundancy, thus five dihedral angles in total. Additionally, the dihedral angle of the C-C bond of the alpha-keto acid group as well as the C-C-O-H bond were both rotated by 180 degrees (2-fold rotation). This generates a total of $3^5 \times 2^2 = 972$ conformers, however the MSTor program deletes any conformer with a smaller interatomic distance than 0.5 \AA by default which resulted in a total of 486 conformers generated. The 486 conformers were then subjected to geometry optimization and harmonic frequency calculations using the DFT functional B3LYP combined with the 6-31+G(d,p) basis set to uncover which conformers were the lowest in energy.¹¹⁵⁻¹¹⁷ Duplicate conformers were identified and removed from the search based on comparing dipole moments and relative energies. A 5 kcal/mol Gibbs energy cutoff relative to the lowest energy conformer was imposed to limit the number of conformers for further analysis. The remaining 68 conformers were re-optimized and had harmonic frequencies calculated using the $\omega\text{B97X-D/may-cc-pVTZ}$ level of theory.¹¹⁸⁻¹²⁰ The $\omega\text{B97X-D}$ functional was chosen because it is one of the better performing global hybrid functionals.^{121,122} Out of these we were left with a total of 66 unique conformers. Harmonic frequencies calculated with the $\omega\text{B97X-D/may-cc-pVTZ}$ method were scaled with a factor of 0.949 to approximate fundamental frequencies which makes spectral assignments more straightforward.^{123,124}

Table 1. Assignment of experimental gas phase vibrational transitions based on calculated frequencies. All frequencies have the units cm^{-1} .

Assignment	Gas Phase Freq.	Solid ATR IR Freq.
OH Stretch	3573/3453	3055
CH_3 Asym Stretch	2971	2955
CH_2 Asym Stretch	2937	2925
CH_3 & CH_2 Sym Stretches	2884	2865
CH_3 & CH_2 Sym stretches	2872	2850
C=O Acid Stretch	1800	1740
C=O Ketone Stretch	1726	1700
CH_3 & CH_2 Sym Bends	1471	1471
CH_3 & CH_2 Sym Bends	1456	1460
C-O-H Bend w/ CH_2 Wag	1375	1375
C-O-H Bend w/ CH_2 Wag	1357	1364
CH_2 Wag	1280	1270
CH_2 Wag	1225	1222
Skeletal C-C Stretch	1128	1125
Mixed Skeletal Modes	1061	1070

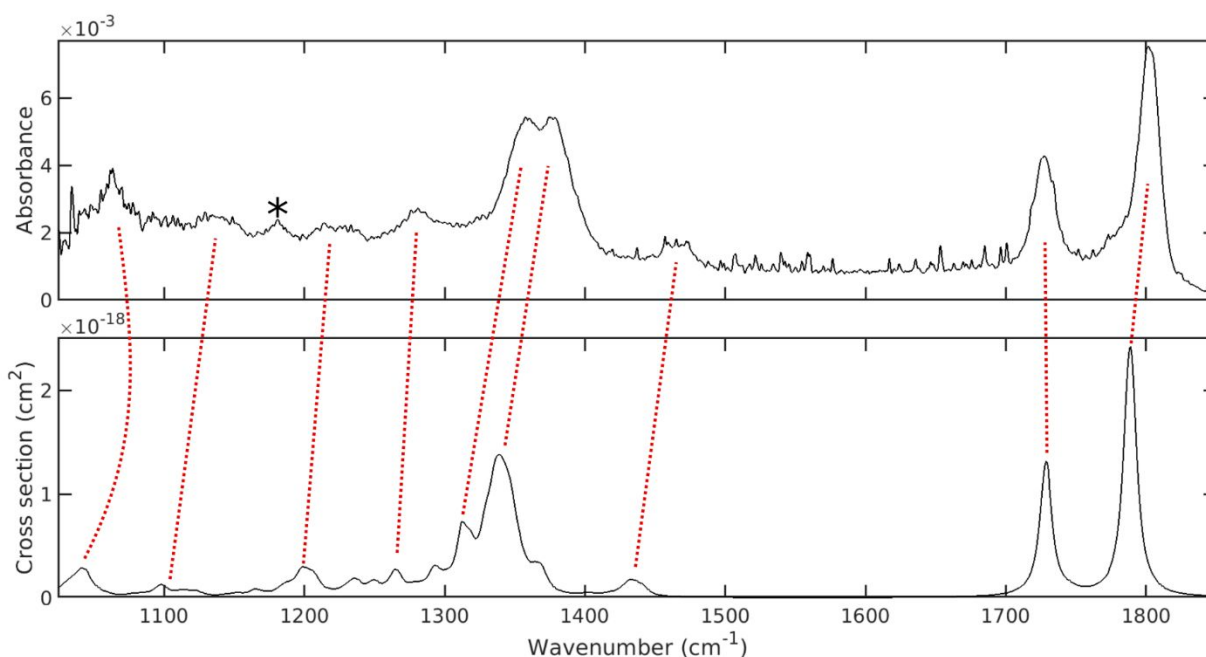


Figure 3. Experimental (top) and calculated (bottom) gas phase IR spectra of 200A. The asterisk denotes a signal assigned to the Tt conformer.

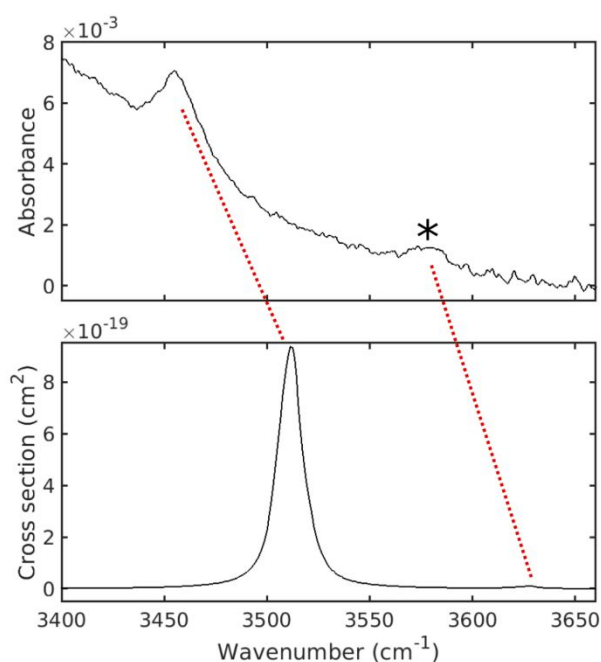


Figure 4. Experimental (top) and calculated (bottom) gas phase IR spectra of 200A in the O-H stretching region. The asterisk denotes a signal assigned to the Tt conformer. The sloping baseline in the experimental spectrum is due to ice formation on the MCT detector.

Results

200A in the Gas Phase. Figures 3-5 show both the calculated and experimental gas phase IR spectrum of 200A in different frequency regions. The calculated spectrum contains contributions from the 66 lowest energy unique conformers and is weighted with their relative calculated abundance such that the lower energy conformers contribute the most. Given the agreement between the experimental and theoretically calculated spectra, it is possible to assign many of the

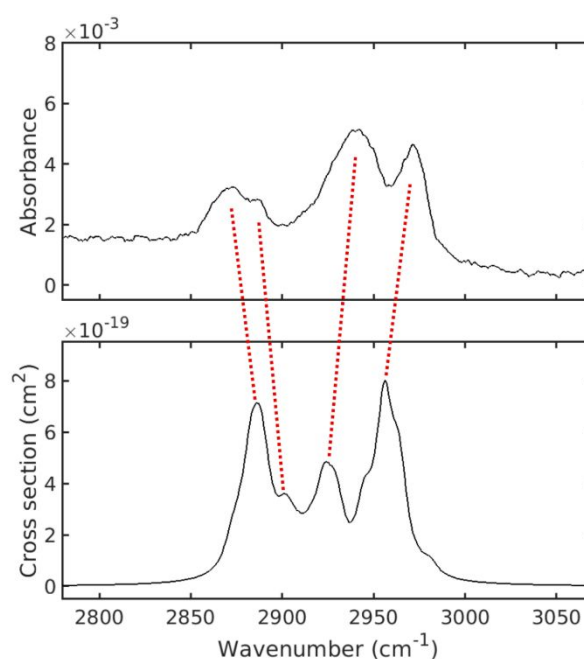


Figure 5. Experimental (top) and calculated (bottom) gas phase IR spectra of 200A in the C-H stretching region.

experimental frequencies to specific vibrational modes (see Table 1).

In addition to several lower energy skeletal modes, some of the more relevant vibrations for this study include the O-H stretching mode which was detected for both the trans-cis (Tc) and trans-trans (Tt) geometries wherein the hydroxyl hydrogen is either H-bonded to the ketonic oxygen (Tc), or is not H-bonded at all (Tt), at 3453 cm^{-1} and 3573 cm^{-1} , respectively. Note that in this work when referring to the Tc and Tt conformers we imply that these labels include all conformations

of the alkyl chain in 200A as individual conformers of varying alkyl chain conformations cannot be distinguished directly in this work. The only spectroscopically distinguishable conformations in this work are indeed only the Tc and Tt variations. An additional transition is identified for the Tt conformers at 1181 cm^{-1} as denoted by an asterisk in Figure 3. The reason these features are not seen in the calculated spectrum is likely due to the computational method overestimating the amount of Tc conformer relative to the amount of Tt conformer in the gas phase. The two peaks assigned to the Tt conformers are based on the computed spectra of the lowest energy Tt conformer see SI Figure S1.

Furthermore, antisymmetric stretching of methyl and methylene groups are observed at 2971 cm^{-1} and 2937 cm^{-1} , while the corresponding symmetric modes are found at 2884 cm^{-1} and 2872 cm^{-1} , respectively. Other prominent features are the acidic and ketonic carbonyl stretches at 1800 cm^{-1} and 1726 cm^{-1} . C-O-H bending with contributions from methylene hydrogen wagging are responsible for the 1375 cm^{-1} and 1357 cm^{-1} peaks while CH_2 wags also give rise to peaks at 1280 cm^{-1} , 1225 cm^{-1} , and 1213 cm^{-1} . Both the experimental and calculated spectra were also used to calculate a saturated vapor pressure for 200A. See the SI for details of the calculation and a comparison to the known saturated vapor pressure of PA.

Table 2. Assignment of ATR vibrational transitions for solid 200A and comparison with corresponding assigned transitions in the gas phase. All frequencies have the units cm^{-1} .

Assignment ^a	Calculated ^b Freq.	Exp. Freq.
Tt OH Stretch	3627	3573
Tc OH Stretch	3511	3453
CH_3 Asym Stretch	2956	2971
CH_2 Asym Stretch	2924	2937
CH_3 & CH_2 Sym Stretches	2902	2884
CH_3 & CH_2 Sym Stretches	2886	2872
C=O Acid Stretch	1789	1800
C=O Ketone Stretch	1728	1726
CH_3 & CH_2 Sym Bends	1433	1471
CH_3 & CH_2 Sym Bends	1402	1456
C-O-H Bend w/ CH_2 Wag ^c	1338	1375
C-O-H Bend w/ CH_2 Wag ^c	1312	1357
CH_2 Wag	1265	1280
CH_2 Wag	1200	1225
CH_2 Wag	$\approx 1187^{\text{d}}$	1213
Tt C-OH Bend	1152	1181
Skeletal C-C Stretch	1098	1128
Mixed Skeletal Mode(s)	1042	1061

^aUnless stated, assignments are attributed to Tc conformers. ^bCalculated frequencies are the peak maxima in the conformer weighted spectra, see Figures 3-5 which use a scale factor of 0.949. ^cSplit due to coupling between C-O-H bend and CH_2 wag. ^dShoulder on the 1200 cm^{-1} peak.

shifted from the gas phase, feature at 3055 cm^{-1} , and the lack of separate bands attributable to Tt and Tc conformers. The methyl and methylene group stretches are slightly red-shifted from the gas phase and are found at 2955 cm^{-1} , 2925 cm^{-1} , 2865 cm^{-1} , and 2850 cm^{-1} . The carbonyl stretches are red-shifted from the gas phase to 1740 cm^{-1} and 1700 cm^{-1} for the acidic and ketonic modes in solid 200A, respectively. A few bands due to methyl and methylene symmetric bends are identified in the spectrum throughout the $1400\text{-}1500\text{ cm}^{-1}$ region. C-O-H bending transitions are observed in the spectrum of solid 200A at 1375 cm^{-1} and 1364 cm^{-1} and this splitting is attributed to coupling with CH_2 wagging. At least two bands due to methylene wags are found at 1270 cm^{-1} and 1222 cm^{-1} .

200A at the Air-Water Interface. IRRAS spectra of 6 mM solutions of 200A were obtained at low (pH=1), unadjusted (pH=2.6), and high (pH=12) pH with both S- and P-polarized light. Table 3 summarizes the features observed under each condition. The left panel in Figure 7 shows a representative S-polarized spectrum in the C-H stretching region for a low pH solution. The peaks at 2960 cm^{-1} , 2930 cm^{-1} , and 2865 cm^{-1} are consistent across pH regimes and polarization. The peak at 2880 cm^{-1} is only observable in the acidic S-polarized spectrum. The sloping baseline is due to ice build-up on the MCT detector and/or evaporation of the water subphase over the course of the experiment, the latter of which is a common phenomenon in IRRAS. In the right panel of Figure 7 the carbonyl stretches are observed as a broad peak spanning from 1750 cm^{-1} to 1680 cm^{-1} in both polarizations with a maximum near 1720 cm^{-1} . Near 1650 cm^{-1} there is a positive feature in the S-polarized spectrum. This feature is not a band due to 200A vibrations, but originates from a surface water bending mode.¹⁰⁸ The left side of Figure 8 shows the carbonyl stretching region of the S-polarized spectra of low and high pH 200A solutions, however that mode is only observable in the low pH regime. In the high pH regime, there is an appreciable depression in the spectra at 1594 cm^{-1} which is ostensibly the COO^- stretch of the anionic species. Neither carbonyl nor carboxylate stretches are observed in the unadjusted pH spectrum. The right side of Figure 8 displays the carbonyl stretch region for PA. There, the bands due to carbonyl stretches are observed between 1750 cm^{-1} and 1660 cm^{-1} in the low pH solutions while the band due to the carboxylate stretch is found at $\approx 1590\text{ cm}^{-1}$ in the high pH solution.

Solid 200A. An ATR transmission spectrum of solid 200A was obtained, shown in Figure 6, and its features are summarized Table 2. Comparison with the assigned gas phase spectrum helps assignment of vibrational transitions in the ATR IR spectrum. Notable differences between gas phase and ATR IR spectra include the hydroxyl hydrogen stretch as a broad, red-

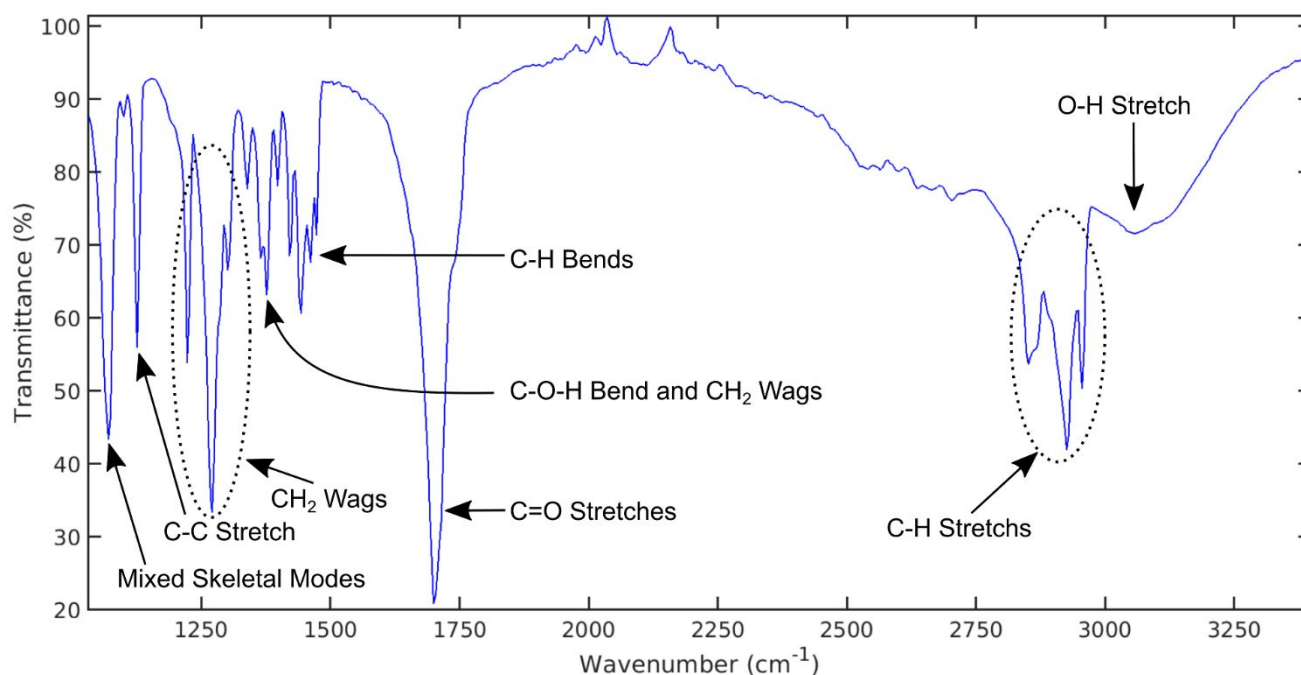


Figure 6. ATR spectrum of solid 200A.

Table 3. Summary of 200A IRRAS spectra. All frequencies have the units cm^{-1} .

Assignment	Gas phase IR	IRRAS S pH=2.6	IRRAS S pH=1	IRRAS P pH=1	IRRAS S pH=12
CH ₃ Asym Stretches	2971	2964, 2960	2960	2956	2963
CH ₂ Asym Stretches	2937	2939	2930	2928	2933
Mixed C-H Sym Stretches	2884, 2872	2879, 2862	2880, 2865	2863	2862
C=O Stretches (Acid, Keto)	1800, 1726		1720	1720	
COO ⁻ Stretch					1594

Discussion

The gas phase conformers of 200A were investigated here and were compared to those for the tailless PA. As Blair *et al.*¹ describe, PA has two conformers seen in the gas phase: Trans-cis (Tc), where the acidic carbonyl is trans to the ketonic carbonyl and the hydroxyl group is cis to the ketonic carbonyl and Trans-trans (Tt), where both the acidic carbonyl and hydroxyl group are trans to the ketonic carbonyl. The Tc conformer is roughly 2 kcal/mol lower in Gibbs energy than Tt and contains a stabilizing intramolecular hydrogen bond between the acidic hydrogen and ketonic carbonyl. Refer to Figure 1 for a visual representation of these conformations in 200A. Blair *et al.*¹ reported that only 3% of the gas phase population of PA exists in the Tt conformer at room temperature and the remainder is in Tc.

For 200A the ω B97X-D/may-cc-pVTZ calculated Gibbs energies suggest that the sum of all Tt conformers make up 2% of the total 200A population. It should be noted here that the mean absolute error with the ω B97X-D functional on conformational

energies is reported to be about 0.7 kcal/mol with a quadruple zeta basis set.¹²¹ Thus while our method is not exactly comparable to the benchmark, that amount of uncertainty in the relative Gibbs energies for the Tc and Tt conformers would give a population range between 0.6% and 6% due to an exponential dependence in the Boltzmann distribution. This is based on a mean average error and not an absolute error, so the actual population range might be larger. Regardless, our calculation of the 200A conformation distribution roughly aligns with the reported PA distribution. We also investigated the integrated experimental absorbances for the OH stretches in the Tc and Tt conformers (See Figure S1 for calculated spectra of Tc vs Tt conformers) as well as the ratio of the corresponding oscillator strengths. However, due to a small impurity in the 200A stock, which contributes to the Tt OH absorption, but not the Tc, and whose other features are likely obscured by the remainder of the 200A spectrum, an accurate experimental ratio between the Tt and Tc conformers could not be obtained for 200A from the IR spectra. See the SI for a brief discussion of the impurity. However, given the agreement between the calculated and experimental 200A IR spectra (Figures 3-5 and

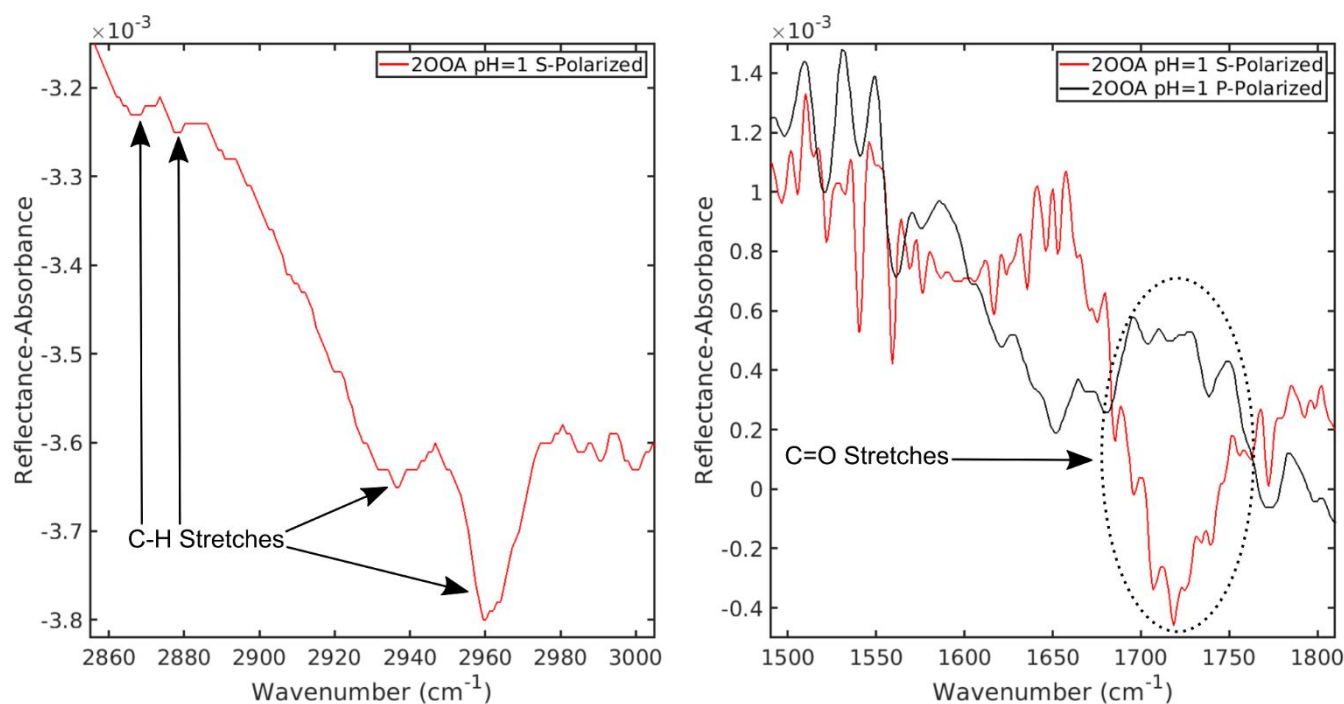


Figure 7. IRRAS spectra of 200A solution at pH=1 in S- (red) and P-(black) polarizations.

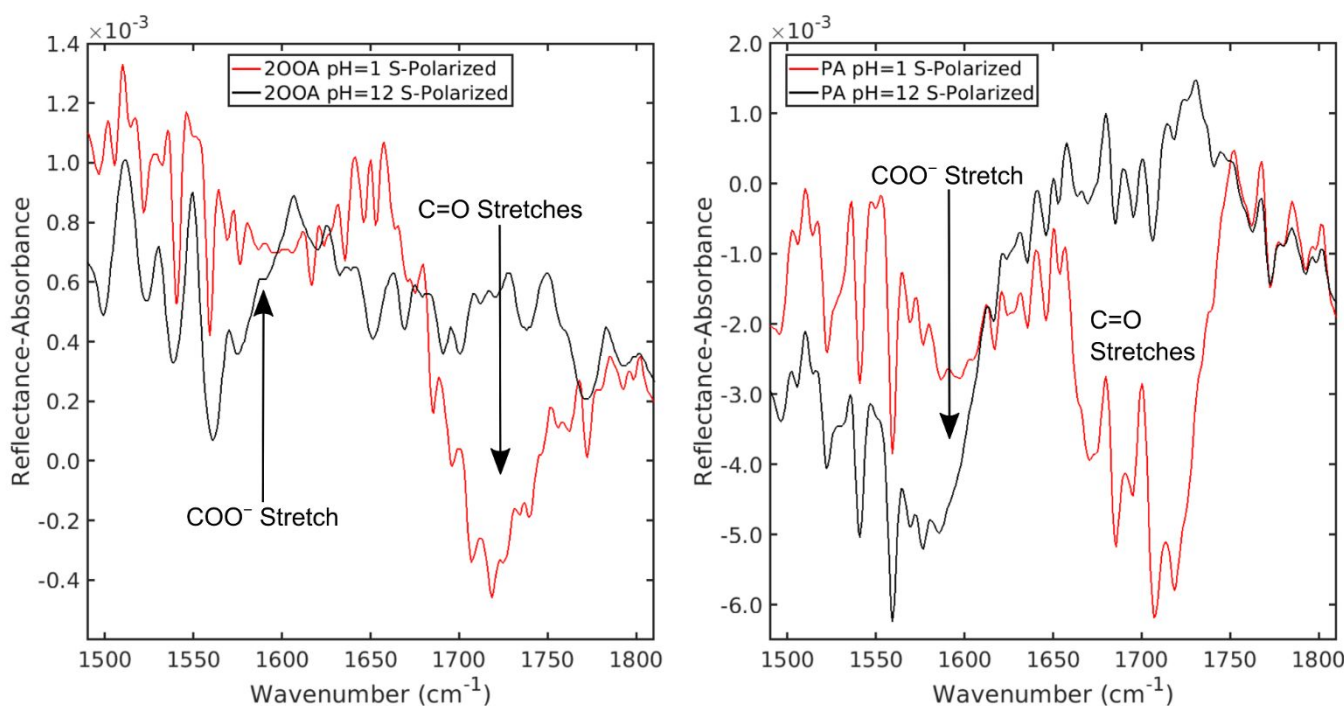


Figure 8. IRRAS spectra of 200A (left) and PA (right) solutions at pH=1 (red) and pH=12 (black) in the S-polarization.

Table 1), and especially the resolution of the two carbonyl stretches and the two OH stretch conformers, we can remain confident in reporting a gas phase 200A spectrum, with the minor caveat that the Tt OH-stretch signal is more intense in the experimental spectrum than expected.

One way the alkyl chain length influences alpha keto acids in the gas phase is by changing the saturated vapor pressure, with

longer chain lengths resulting in lower saturated vapor pressures. Indeed, in this work we found that 2OOA has a saturated vapor pressure between 2 mTorr and 20 mTorr at ambient conditions, which is significantly lower than for PA at 1 Torr.¹²⁵ See the SI for details of the calculation.¹²⁶⁻¹²⁸ Thus, alkyl chain lengths will significantly impact where and in which quantities any fatty acid will be found in the environment thereby influencing the reactions available to and longevity of each fatty acid in the environment.

Surface specific vibrational spectroscopy has been used in the literature to determine molecular structure, orientation, and conformation of film-forming surfactants at the air-water interface.^{87,129-131} For fatty acids, the antisymmetric and symmetric CH₂ stretch frequencies in the hydrocarbon are used to describe the ordering of molecules in a film. A highly ordered fatty acid film is comprised of molecules whose hydrocarbon tails are in the all *trans* conformation, allowing the tails to align perpendicularly to the water surface. The hydrocarbon tails are forced into the all *trans* conformation when there is relatively strong intermolecular interaction amongst the aliphatic tails and that interaction is signified spectroscopically by a lower CH₂ stretch frequency. On the other hand, when there are fewer interactions available between the hydrocarbon tails, the CH₂ stretch frequency will be higher as the tails are allowed to adopt any number of *gauche* conformations.^{130,131} We apply those same principles to the 2OOA IRRAS spectra presented here and compare them with the gas and solid phase IR spectra recorded in this work.

As summarized in Table 4, in the gas phase the antisymmetric CH₂ stretch is observed at 2937 cm⁻¹ compared to 2925 cm⁻¹ for solid 2OOA, and 2930 cm⁻¹ across the different pH levels in the IRRAS spectra. As expected, gas phase 2OOA has the highest energy $\nu_a(\text{CH}_2)$ and therefore the least amount of Van der Waals interactions between molecules. Van der Waals interactions between closely packed alkyl tails lowers the energy of the $\nu_a(\text{CH}_2)$ for solid 2OOA.

Table 4. Summary of selected vibrational frequencies assigned to 2OOA across multiple phases. All frequencies have units of cm⁻¹.

Mode	Gas phase	Air-Water Interface	Solid phase
Antisymmetric CH ₂ stretch	2937	2930	2925
Carbonyl Stretches	1800/1726	1720	1740/1700

We also observe significant red shifting in the OH stretch for the solid compared to gas phase. Blair *et al.*¹ calculated that the OH stretches of a PA dimer should red shift by ≈ 500 cm⁻¹ to an absolute wavenumber which is ≈ 100 cm⁻¹ higher energy than the methyl stretches compared to monomers of PA in gas phase. We observed a similar shift for 2OOA where the OH stretches are represented by a broad peak around 3055 cm⁻¹ in the solid compared to 3573 cm⁻¹ and 3453 cm⁻¹ in the gas phase. The agreement between theoretically predicted and experimentally measured shifts for a PA dimer and 2OOA solid

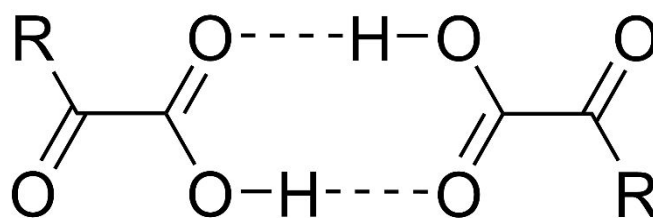


Figure 9. Sketch of an alpha-keto acid dimeric structure.

allows us to use the PA dimer as a model for the polar headgroup in the solid phase 2OOA.

Overall, by comparing the CH₂ stretching frequency between 2OOA in different phases, we develop a picture of the relative level of molecular ordering. In the gas phase, where the 2OOA hydrocarbon tail can exist in many conformers without intermolecular interactions constricting it, the methylene stretches have a relatively high transition energy whereas in solid 2OOA, the transition energy is lower since the molecules are more tightly packed. At the interface, the 2OOA tails do exhibit some interaction with each other and the several wavenumber redshift from the gas phase is indicative of a "significant"¹³² decrease in *gauche* conformations in the alkyl chain. This is an important result that demonstrates soluble oxoacids having enough surface activity to partition from the bulk to align and interact with each other at the air-water interface.

Just as the C-H stretches of hydrocarbon tails have been used to investigate the orientation, conformation, and packing of fatty acids on the surface of water,^{87,129-131} the carbonyl stretching frequency can reveal similar information.¹²⁹ In a typical view of amphiphilic species residing at a water surface the hydrophilic head group is in contact with the water subphase while the hydrophobic tail faces away from the water subphase. As such, the C=O groups are susceptible to hydrogen bonding with water and potentially neighboring surfactant molecules. Previous studies on interfacial fatty acids were able to resolve 3 different carbonyl stretch frequencies derived from 3 different hydrogen bonding environments and were then able to identify the molecular conformation and implied level of packing.^{95,129} While our experiments do not allow us to resolve individual conformers, partially due to the additional carbonyl group and the convolution of the acidic and ketonic carbonyl stretches in the IRRAS spectra, there is still an interesting comparison to be made between the different environments.

As summarized in Table 4, in the gas phase the 2OOA carbonyl stretches exist at 1800 cm⁻¹ and 1726 cm⁻¹ for the acid and keto $\nu(\text{C=O})$, respectively. In the solid there is one feature at 1700 cm⁻¹ with a shoulder at 1740 cm⁻¹, and at the air/water interface there is a single, broad feature spanning ≈ 1750 -1680 cm⁻¹ with a maximum near 1720 cm⁻¹. In the gas phase no evidence of intermolecularly hydrogen bonded 2OOA is observed in our spectra and therefore the monomeric 2OOA C=O transition frequencies are generally higher in energy compared to the other environments investigated in this work.

However, the dominant gas phase conformer in our spectra is Tc 2OOA in which the hydroxyl hydrogen is H-bonded with the ketonic oxygen. As such, the Tc keto $\nu(\text{C}=\text{O})$ is red-shifted compared to an alpha keto $\nu(\text{C}=\text{O})$ that does not hydrogen bond. In our calculated spectrum, the red-shift is 24 cm^{-1} from the Tt to Tc keto $\nu(\text{C}=\text{O})$ so the experimental Tt keto $\nu(\text{C}=\text{O})$ is likely obscured by the acidic $\nu(\text{C}=\text{O})$ near 1750 cm^{-1} .

For solid phase 2OOA, there is a single major OH stretch feature that is significantly red-shifted from the gas phase due to the intermolecular hydrogen bonding allowed by the close packing of molecules as a solid. This corroborates our analysis of the C-H stretching region. In solid 2OOA the main absorbance at 1700 cm^{-1} is due to the carboxylic acid carbonyl hydrogen bonding intermolecularly to another carboxylic acid OH group. This acid-acid group hydrogen bonding scheme shown in Figure 9 is a highly favorable hydrogen bonding arrangement¹³³⁻¹³⁶ and it was calculated for the pyruvic acid dimer that this results in a red shift of 83 cm^{-1} of the acidic carbonyl stretch transition frequency compared to the Tc monomer. In this arrangement, the keto carbonyl may be able to hydrogen bond with neighboring acid groups, but the availability of hydrogen bond donor groups is limited given that the molecule contains only one donor group and two acceptor groups, and the acid-acid hydrogen bonded arrangement is energetically favorable. Therefore, we assign the shoulder at 1740 cm^{-1} to the $\nu(\text{C}=\text{O})_{\text{keto}}$ which is 14 cm^{-1} blue shifted compared to the intramolecularly hydrogen bonded Tc $\nu(\text{C}=\text{O})_{\text{keto}}$ in the gas phase.

We were not able to distinguish the ketonic and acidic carbonyl stretches in the IRRAS spectra and the approximately 70 cm^{-1} width of the carbonyl signature vibration may imply there are multiple conformations or hydrogen bonding environments contributing to that feature. See Figure 10 for a schematic representation of some of the possible environments. The highest energy end of the absorption (1750 cm^{-1}) matches our estimate for the frequency of a non-hydrogen bonded $\nu(\text{C}=\text{O})_{\text{keto}}$ which could occur if the OH group of 2OOA is pointed into bulk. The acidic carbonyl would then orient itself predominantly along the interface, and the ketonic carbonyl would be close to parallel with, and above the interface. This orientation would more likely occur when the hydrocarbon tail is in an all *trans* conformation, and our analysis of the CH stretch region suggests that there are significantly fewer gauche conformations at the interface than in the solid or gas phase. At approximately 1680 cm^{-1} the frequency is even lower than the $\nu(\text{C}=\text{O})_{\text{keto}}$ of solid 2OOA. Muro *et al.*¹²⁹ showed that interfacial fatty acids exhibit lower energy acidic carbonyl vibrational transitions when both the carbonyl and hydroxyl groups point into the bulk. This is an orientation that occurs when a gauche conformation in the tail is present near the acid group, and the molecules are packed tightly enough together to hydrogen bond with each other, forming an intermolecular H-bond network. Applying that to alpha keto acids, the ketone would be angled away from the bulk but is ostensibly still deep enough to participate in hydrogen bonding with subphase water. However, the maximum of the absorbance is near 1720 cm^{-1}

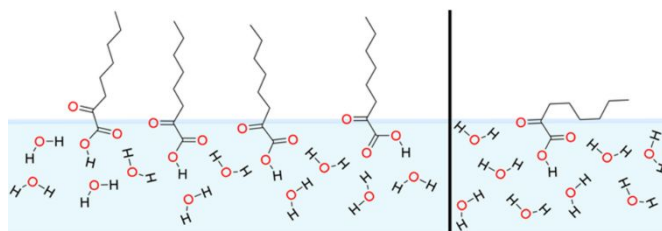


Figure 10. A schematic representation of possible orientations and hydrogen bonding environments of interfacial 2OOA.

which is of relatively high energy for a carbonyl stretch in an environment where multiple hydrogen bonds to the carbonyl are possible and the transition frequency is close to the frequency of the singly hydrogen bonded $\nu(\text{C}=\text{O})_{\text{keto}}$ of the gas phase Tc conformer. The intermediate position within the absorption also fits with the Gericke and Hühnerfuss⁹⁵ protonation model of the carbonyl being monoprotonated and with the Muro *et al.*¹²⁹ idea of the bond being hydrated but not participating in an intermolecular hydrogen bond network. Furthermore, the frequency matches other assignments of carbonyl stretches in interfacial lipids¹³⁷. Applied to alpha keto acids, the molecule would be sitting as described just above, but the polar head group would have to sit deep enough in the water to allow the keto carbonyl to hydrogen bond with water. 2OOA sitting with its polar head group in the water, allowing for hydrogen bonding with water, but not being close enough to other molecules to participate in additional intermolecular H-bonding is perhaps the most intuitive picture based on its amphiphilic character yet slightly soluble nature. As such, 2OOA molecules at the air-water interface may be close enough together for their alkyl tails to interact and provide some ordering, but not to the same level as in solid 2OOA as shown by the relative C-H vibrational shifts. They are not so densely packed, however, that their headgroups also interact with each other, which would further lower the energy of the carbonyl stretch transitions.

The carbonyl stretching modes in 2OOA can be compared to those in PA to elucidate the effect of tail length, and presumed surface ordering, may have on those vibrations. As seen in Figure 8, the frequency and shape of the IRRAS C=O feature is largely the same for PA and 2OOA. It is therefore likely that water is the main supplier of hydrogen bonds to alpha keto acids at the air-water interface, and that the packing is either not dense enough or energetically favorable enough to support intermolecular hydrogen bonding between alpha keto acids.

Conclusions

We have investigated the vibrational spectrum of 2OOA in three phases: the gas phase, solid phase, and at the air-water interface. With computational support, we assigned many of the experimental features to specific vibrational modes. We focused on the C-H stretch and C=O stretch regions to compare how 2OOA interacts with its surroundings in each environment, with specific attention paid to the surface of water. At the air-

water interface intermolecular interactions occur between neighbouring alkyl tails. The C=O stretching fundamental transition frequency indicates that the carbonyls mainly participate in hydrogen bonding with water, but the molecules do not directly hydrogen bond with each other as they do in solid 2OOA. Overall, these results provide a picture of interfacial 2OOA with the polar headgroup with both carbonyl groups interacting with the water subphase and with their hydrophobic tails in a mostly trans conformation pointing away from the surface.

We also compared the 2OOA spectra in each phase to the analogous PA spectrum to investigate the effect alpha-keto acid tail length has on their inter- and intra-molecular interactions. In the gas phase, beyond the calculated ≈ 2 order of magnitude difference in saturated vapor pressure, the tail does not significantly affect the spectral signatures from the 2-oxo acid headgroup. The relative abundances of the Tt and Tc conformers for each molecule are similar as well. As a solid, we proposed a hydrogen bonding scheme for closely packed 2OOA headgroups, which is based on the PA dimer. At the air-water interface, where the longer tail of 2OOA contributed significant hydrophobicity relative to PA, the alkyl tail length did not appear to manifest a difference in the hydrogen bonding environment of the carbonyl groups for each molecule. However, if as proposed, water is the main contributor of hydrogen bonds to alpha-keto acid carbonyls, the surface of a 2OOA solution may still look different than a PA solution as the tail length influences the overall solubility of the molecule. Similarly, in the natural environment, the longer tailed alpha-keto acids will preferentially be found on the surface of atmospheric particles and in the sea-surface microlayer.

Conflicts of interest

There are no conflicts to declare.

Acknowledgements

This work was funded by the U. S. Army Research Office, grant #ARO W911NF1710115, and the National Science Foundation, grant #CHE 1611107. B.N.F acknowledges funding from the Independent Research Fund, Denmark, grant #9056-00005B.

Notes and references

- 1 S. L. Blair, A. E. R. Harris, B. N. Frandsen, H. G. Kjaergaard, E. Pangui, M. Cazaunau, J. F. Doussin and V. Vaida, *J. Phys. Chem. A*, 2020, **124**, 1240-1252.
- 2 K. L. Plath, K. Takahashi, R. T. Skodje and V. Vaida, *J. Phys. Chem. A*, 2009, **113**, 7294-7303.
- 3 A. E. R. Harris, M. Cazaunau, A. Gratien, E. Pangui, J. F. Doussin and V. Vaida, *J. Phys. Chem. A*, 2017, **121**, 8348-8358.
- 4 A. E. Reed Harris, J. F. Doussin, B. K. Carpenter and V. Vaida, *J. Phys. Chem. A*, 2016, **120**, 10123-10133.
- 5 A. E. Reed Harris, A. Pajunoja, M. Cazaunau, A. Gratien, E. Pangui, A. Monod, E. C. Griffith, A. Virtanen, J. F. Doussin and V. Vaida, *J. Phys. Chem. A*, 2017, **121**, 3327-3339.
- 6 J. R. Church, V. Vaida and R. T. Skodje, *J. Phys. Chem. A*, 2020, **124**, 790-800.
- 7 J. R. Church, PhD Thesis, University of Colorado Boulder, 2018.
- 8 M. O. Andreae, R. W. Talbot and S. M. Li, *J. Geophys. Res.: Atmos.*, 1987, **92**, 6635-6641.
- 9 P. G. Eger, J. Schuladen, N. Sobanski, H. Fischer, E. Karu, J. Williams, M. Riva, Q. Zha, M. Ehn and L. L. Quéléver, *Atmos. Chem. Phys.*, 2020, **20**, 3697-3711.
- 10 M. Guzmán, M. Hoffmann and A. Colussi, *J. Geophys. Res.: Atmos.*, 2007, **112**, D10123.
- 11 M. Shiraiwa, A. Zuend, A. K. Bertram and J. H. Seinfeld, *Phys. Chem. Chem. Phys.*, 2013, **15**, 11441-11453.
- 12 B. Ervens, *Chem. Rev.*, 2015, **115**, 4157-4198.
- 13 B. Ervens, A. G. Carlton, B. J. Turpin, K. E. Altieri, S. M. Kreidenweis and G. Feingold, *Geophys. Res. Lett.*, 2008, **35**, 11069-11102.
- 14 B. Ervens, S. Gligorovski and H. Herrmann, *Phys. Chem. Chem. Phys.*, 2003, **5**, 1811-1824.
- 15 B. Ervens, B. J. Turpin and R. J. Weber, *Atmos. Chem. Phys.*, 2011, **11**, 11069-11102.
- 16 A. Mellouki and Y. Mu, *J. Photochem. Photobiol., A*, 2003, **157**, 295-300.
- 17 M. G. Berges and P. Warneck, *Berichte der Bunsengesellschaft für Physikalische Chemie*, 1992, **96**, 413-416.
- 18 D. Grosjean, *Atmos. Environ. (1967-1989)*, 1983, **17**, 2379-2382.
- 19 P. A. Leermakers and G. F. Vesley, *J. Am. Chem. Soc.*, 1963, **85**, 3776-3779.
- 20 S. Sutradhar, B. R. Samanta, R. Fernando and H. Reisler, *J. Phys. Chem. A*, 2019, **123**, 5906-5917.
- 21 K. Takahashi, K. L. Plath, R. T. Skodje and V. Vaida, *J. Phys. Chem. A*, 2008, **112**, 7321-7331.
- 22 G. F. Vesley and P. A. Leermakers, *J. Phys. Chem.*, 1964, **68**, 2364-2366.
- 23 S. Yamamoto and R. A. Back, *Can. J. Chem.*, 1985, **63**, 549-554.
- 24 X.-P. Chang, Q. Fang and G. Cui, *J. Chem. Phys.*, 2014, **141**, 154311.
- 25 G. da Silva, *J. Phys. Chem. A*, 2016, **120**, 276-283.
- 26 I. D. Reva, S. G. Stepanian, L. Adamowicz and R. Fausto, *J. Phys. Chem. A*, 2001, **105**, 4773-4780.
- 27 D. Gerbig and P. R. Schreiner, *J. Phys. Chem. B*, 2015, **119**, 693-703.
- 28 V. Barone, M. Biczysko, J. Bloino, P. Cimino, E. Penocchio and C. Puzzarini, *J. Chem. Theory Comput.*, 2015, **11**, 4342-4363.
- 29 G. Buemi, *J. Phys. Org. Chem.*, 2009, **22**, 933-947.
- 30 C. Chen and S.-F. Shyu, *J. Mol. Struct.: THEOCHEM*, 2000, **503**, 201-211.
- 31 M. K. Maroń, K. Takahashi, R. K. Shoemaker and V. Vaida, *Chem. Phys. Lett.*, 2011, **513**, 184-190.
- 32 K. E. Norris, G. B. Bacskay and J. E. Gready, *J. Comput. Chem.*, 1993, **14**, 699-714.
- 33 I. Reva, C. M. Nunes, M. Biczysko and R. Fausto, *J. Phys. Chem. A*, 2015, **119**, 2614-2627.
- 34 A. J. Eugene and M. I. Guzman, *J. Phys. Chem. A*, 2017, **121**, 2924-2935.
- 35 A. J. Eugene and M. I. Guzman, *Molecules*, 2019, **24**, 1124-1135.
- 36 E. C. Griffith, B. K. Carpenter, R. K. Shoemaker and V. Vaida, *Proc. Natl. Acad. Sci. U. S. A.*, 2013, **110**, 11714-11719.

- 37 E. C. Griffith, B. K. Carpenter, R. K. Shoemaker and V. Vaida, *Proc. Natl. Acad. Sci. U. S. A.*, 2013, **110**, E4276-E4276.
- 38 E. C. Griffith, R. J. Rapf, R. K. Shoemaker, B. K. Carpenter and V. Vaida, *J. Am. Chem. Soc.*, 2014, **136**, 3784-3787.
- 39 E. C. Griffith, R. K. Shoemaker and V. Vaida, *Origins Life Evol. Biospheres*, 2013, **43**, 341-352.
- 40 M. Guzman, A. Colussi and M. Hoffmann, *J. Phys. Chem. A*, 2006, **110**, 3619-3626.
- 41 M. C. Larsen and V. Vaida, *J. Phys. Chem. A*, 2012, **116**, 5840-5846.
- 42 P. Leermakers and G. Vesley, *J. Org. Chem.*, 1963, **28**, 1160.
- 43 M. Mekić, M. Brigante, D. Vione and S. Gligorovski, *Atmos. Environ.*, 2018, **185**, 237-242.
- 44 R. J. Rapf, R. J. Perkins, B. K. Carpenter and V. Vaida, *J. Phys. Chem. A*, 2017, **121**, 4272-4282.
- 45 R. J. Rapf, R. J. Perkins, H. S. Yang, G. Miyake, B. K. Carpenter and V. Vaida, *J. Am. Chem. Soc.*, 2017, **139**, 6946-6959.
- 46 C. J. Ebben, B. F. Strick, M. A. Upshur, H. M. Chase, J. L. Achtyl, R. J. Thomson and F. M. Geiger, *Atmos. Chem. Phys.*, 2014, **14**, 2303-2314.
- 47 J. H. Seinfeld and S. N. Pandis, *Atmospheric Chemistry and Physics: from Air Pollution to Climate Change*, John Wiley & Sons, Hoboken, New Jersey, 2016.
- 48 V. Masson-Delmotte, P. Zhai, A. Pirani, S. L. Connors, C. Péan, S. Berger, N. Caud, Y. Chen, L. Goldfarb, M. I. Gomis, M. Huang, K. Leitzell, E. Lonnoy, J. B. R. Matthews, T. K. Maycock, T. Waterfield, O. Yelekçi, R. Yu, and B. Zhou (eds.), *IPCC, 2021: Summary for Policymakers. In: Climate Change 2021: The Physical Science Basis. Contribution of Working Group I to the Sixth Assessment Report of the Intergovernmental Panel on Climate Change* Cambridge University Press.
- 49 E. C. Griffith, A. F. Tuck and V. Vaida, *Acc. Chem. Res.*, 2012, **45**, 2106-2113.
- 50 C. M. Dobson, G. B. Ellison, A. F. Tuck and V. Vaida, *Proc. Natl. Acad. Sci. U. S. A.*, 2000, **97**, 11864-11868.
- 51 D. J. Donaldson and V. Vaida, *Chem. Rev.*, 2006, **106**, 1445-1461.
- 52 S. Banerjee, E. Gnanamani, X. Yan and R. N. Zare, *Analyst (Cambridge, U. K.)*, 2017, **142**, 1399-1402.
- 53 C. F. Chamberlayne and R. N. Zare, *J. Chem. Phys.*, 2020, **152**, 184702.
- 54 G. B. Ellison, A. F. Tuck and V. Vaida, *J. Geophys. Res.: Atmos.*, 1999, **104**, 11633-11641.
- 55 C. George, M. Ammann, B. D'Anna, D. J. Donaldson and S. A. Nizkorodov, *Chem. Rev.*, 2015, **115**, 4218-4258.
- 56 E. C. Griffith and V. Vaida, *Proc. Natl. Acad. Sci. U. S. A.*, 2012, **109**, 15697-15701.
- 57 E. C. Griffith and V. Vaida, *J. Am. Chem. Soc.*, 2013, **135**, 710-716.
- 58 K. J. Kappes, A. M. Deal, M. F. Jespersen, S. L. Blair, J.-F. Doussin, M. Cazaunau, E. Pangui, B. N. Hopper, M. S. Johnson and V. Vaida, *J. Phys. Chem. A*, 2021, **125**, 1036-1049.
- 59 J. K. Lee, S. Banerjee, H. G. Nam and R. N. Zare, *Q. Rev. Biophys.*, 2015, **48**, 437-444.
- 60 J. K. Lee, D. Samanta, H. G. Nam and R. N. Zare, *J. Am. Chem. Soc.*, 2019, **141**, 10585-10589.
- 61 J. K. Lee, K. L. Walker, H. S. Han, J. Kang, F. B. Prinz, R. M. Waymouth, H. G. Nam and R. N. Zare, *Proc. Natl. Acad. Sci. U. S. A.*, 2019, **116**, 19294-19298.
- 62 B. M. Marsh, K. Iyer and R. G. Cooks, *J. Am. Soc. Mass Spectrom.*, 2019, **30**, 2022-2030.
- 63 I. Nam, J. K. Lee, H. G. Nam and R. N. Zare, *Proc. Natl. Acad. Sci. U. S. A.*, 2017, **114**, 12396-12400.
- 64 S. Rossignol, L. Tinel, A. Bianco, M. Passananti, M. Brigante, D. J. Donaldson and C. George, *Science*, 2016, **353**, 699-702.
- 65 M. F. Ruiz-Lopez, J. S. Francisco, M. T. Martins-Costa and J. M. Anglada, *Nat. Rev. Chem.*, 2020, **4**, 459-475.
- 66 H. Q. Xiong, J. K. Lee, R. N. Zare and W. Min, *J. Phys. Chem. Lett.*, 2020, **11**, 7423-7428.
- 67 J. Zhong, M. Kumar, J. M. Anglada, M. T. C. Martins-Costa, M. F. Ruiz-Lòpez, X. C. Zeng and J. S. Francisco, *Annu. Rev. Phys. Chem.*, 2019, **70**, 45-69.
- 68 Y. Jung and R. Marcus, *J. Am. Chem. Soc.*, 2007, **129**, 5492-5502.
- 69 Z. Wei, Y. Li, R. G. Cooks and X. Yan, *Annu. Rev. Phys. Chem.*, 2020, **71**, 31-51.
- 70 M. Ahmed, M. Blum, E. J. Crumlin, P. L. Geissler, T. Head-Gordon, D. T. Limmer, K. K. Mandadapu, R. J. Saykally and K. R. Wilson, *J. Phys. Chem. B*, 2021, **125**, 9037-9051.
- 71 K. R. Wilson, A. M. Prophet, G. Rovelli, M. D. Willis, R. J. Rapf and M. I. Jacobs, *Chem. Sci.*, 2020, **11**, 8533-8545.
- 72 E. Benichou, A. Bruyère, E. Forel, O. Bonhomme and P.-F. Brevet, *Organic Photonic Materials and Devices XVII*, SPIE, Bellingham, Washington USA, 2015.
- 73 W.-k. Zhang, D.-s. Zheng, Y.-y. Xu, H.-t. Bian, Y. Guo and H.-f. Wang, *J. Chem. Phys.*, 2005, **123**, 224713.
- 74 K. Sahu, K. B. Eisenthal and V. F. McNeill, *J. Phys. Chem. C*, 2011, **115**, 9701-9705.
- 75 A. Beloqui Redondo, I. Jordan, I. Ziazadeh, A. Kleibert, J. B. Giorgi, H. J. Wörner, S. May, Z. Abbas and M. A. Brown, *J. Phys. Chem. C*, 2015, **119**, 2661-2668.
- 76 Q. Sun and Y. Guo, *J. Mol. Liq.*, 2016, **213**, 28-32.
- 77 A. P. Ault, D. Zhao, C. J. Ebben, M. J. Tauber, F. M. Geiger, K. A. Prather and V. H. Grassian, *Phys. Chem. Chem. Phys.*, 2013, **15**, 6206-6214.
- 78 C. J. Ebben, A. P. Ault, M. J. Ruppel, O. S. Ryder, T. H. Bertram, V. H. Grassian, K. A. Prather and F. M. Geiger, *J. Phys. Chem. A*, 2013, **117**, 6589-6601.
- 79 K. Eisenthal, *Chem. Rev.*, 1996, **96**, 1343-1360.
- 80 B. P. Gordon, F. G. Moore, L. F. Scatena and G. L. Richmond, *J. Phys. Chem. A*, 2019, **123**, 10609-10619.
- 81 W. Liu, Z. Wang, L. Fu, R. M. Leblanc and E. C. Y. Yan, *Langmuir*, 2013, **29**, 15022-15031.
- 82 G. R. Medders and F. Paesani, *J. Am. Chem. Soc.*, 2016, **138**, 3912-3919.
- 83 A. Morita and J. T. Hynes, *Chem. Phys.*, 2000, **258**, 371-390.
- 84 S. K. Reddy, R. Thiriaux, B. A. W. Rudd, L. Lin, T. Adel, T. Joutsuka, F. M. Geiger, H. C. Allen, A. Morita and F. Paesani, *Chem*, 2018, **4**, 1629-1644.
- 85 G. Richmond, *Chem. Rev.*, 2002, **102**, 2693-2724.
- 86 Y. R. Shen and V. Ostroverkhov, *Chem. Rev.*, 2006, **106**, 1140-1154.
- 87 C. Y. Tang, Z. Huang and H. C. Allen, *J. Phys. Chem. B*, 2010, **114**, 17068-17076.
- 88 D. Verreault, W. Hua and H. C. Allen, *J. Phys. Chem. Lett.*, 2012, **3**, 3012-3028.
- 89 E. C. Y. Yan, L. Fu, Z. Wang and W. Liu, *Chem. Rev.*, 2014, **114**, 8471-8498.
- 90 D. Blaudez, T. Buffeteau, J. C. Cornut, B. Desbat, N. Escafre, M. Pezolet and J. M. Turlet, *J. Appl. Spectrosc.*, 1993, **47**, 869-874.
- 91 D. Blaudez, S. Castano and B. Desbat, in *Biointerface Characterization by Advanced IR Spectroscopy*, ed. C. M. Pradier and Y. J. Chabal, Elsevier, Amsterdam, 1st Edition, 2011, Chapter 2, 27-55.
- 92 R. A. Dluhy, *J. Phys. Chem.*, 1986, **90**, 1373-1379.
- 93 R. A. Dluhy, *Appl. Spectrosc. Rev.*, 2000, **35**, 315-351.
- 94 A. Gericke, J. Brauner, R. Erukulla, R. Bittman and R. Mendelsohn, *Thin Solid Films*, 1996, **284**, 428-431.

- 95 A. Gericke and H. Huehnerfuss, *J. Phys. Chem.*, 1993, **97**, 12899-12908.
- 96 A. Gericke, A. V. Michailov and H. Hühnerfuss, *Vib. Spectrosc.*, 1993, **4**, 335-348.
- 97 S. Gopalakrishnan, D. F. Liu, H. C. Allen, M. Kuo and M. J. Shultz, *Chem. Rev.*, 2006, **106**, 1155-1175.
- 98 M. B. Meinders, G. G. van den Bosch and H. H. de Jongh, *Eur. Biophys. J.*, 2001, **30**, 256-267.
- 99 A. Meister, A. Kerth and A. Blume, *J. Phys. Chem. B*, 2005, **109**, 6239-6246.
- 100 R. Mendelsohn, J. W. Brauner and A. Gericke, *Annu. Rev. Phys. Chem.*, 1995, **46**, 305-334.
- 101 M. Shrestha, M. Luo, Y. Li, B. Xiang, W. Xiong and V. H. Grassian, *Chem. Sci.*, 2018, **9**, 5716-5723.
- 102 C. D. Bain, P. B. Davies, T. H. Ong, R. N. Ward and M. A. Brown, *Langmuir*, 1991, **7**, 1563-1566.
- 103 Y. Wang, X. Du, L. Guo and H. Liu, *J. Chem. Phys.*, 2006, **124**, 134706.
- 104 R. Mendelsohn, G. Mao and C. R. Flach, *Biochim. Biophys. Acta, Biomembr.*, 2010, **1798**, 788-800.
- 105 M. Handke, M. Milosevic and N. Harrick, *Vib. Spectrosc.*, 1991, **1**, 251-262.
- 106 K. Yamamoto and H. Ishida, *Vib. Spectrosc.*, 1994, **8**, 1-36.
- 107 T. Hasegawa, S. Takeda, A. Kawaguchi and J. Umemura, *Langmuir*, 1995, **11**, 1236-1243.
- 108 C. R. Flach, A. Gericke and R. Mendelsohn, *J. Phys. Chem. B*, 1997, **101**, 58-65.
- 109 A. Gericke, J. Simon-Kutscher and H. Huehnerfuss, *Langmuir*, 1993, **9**, 3115-3121.
- 110 S. Li, L. Du, Z. Wei and W. Wang, *Sci. Total Environ.*, 2017, **580**, 1155-1161.
- 111 V. P. Tolstoy, I. Chernyshova and V. A. Skryshevsky, *Handbook of Infrared Spectroscopy of Ultrathin Films*, John Wiley & Sons, Hoboken, New Jersey, 2003.
- 112 M. J. Frisch, G. W. Trucks, H. B. Schlegel, G. E. Scuseria, M. A. Robb, J. R. Cheeseman, G. Scalmani, V. Barone, G. A. Petersson, H. Nakatsuji, X. Li, M. Caricato, A. V. Marenich, J. Bloino, B. G. Janesko, R. Gomperts, B. Mennucci, H. P. Hratchian, J. V. Ortiz, A. F. Izmaylov, J. L. Sonnenberg, Williams, F. Ding, F. Lipparini, F. Egidi, J. Goings, B. Peng, A. Petrone, T. Henderson, D. Ranasinghe, V. G. Zakrzewski, J. Gao, N. Rega, G. Zheng, W. Liang, M. Hada, M. Ehara, K. Toyota, R. Fukuda, J. Hasegawa, M. Ishida, T. Nakajima, Y. Honda, O. Kitao, H. Nakai, T. Vreven, K. Throssell, J. A. Montgomery Jr., J. E. Peralta, F. Ogliaro, M. J. Bearpark, J. J. Heyd, E. N. Brothers, K. N. Kudin, V. N. Staroverov, T. A. Keith, R. Kobayashi, J. Normand, K. Raghavachari, A. P. Rendell, J. C. Burant, S. S. Iyengar, J. Tomasi, M. Cossi, J. M. Millam, M. Klene, C. Adamo, R. Cammi, J. W. Ochterski, R. L. Martin, K. Morokuma, O. Farkas, J. B. Foresman and D. J. Fox, *Gaussian 16 Rev. A.03*, Gaussian Inc., Wallingford CT, 2016.
- 113 J. Zheng, S. L. Mielke, K. L. Clarkson and D. G. Truhlar, *Comput. Phys. Commun.*, 2012, **183**, 1803-1812.
- 114 J. Zheng, S. L. Mielke, J. L. Bao, R. Meana-Pañeda, K. L. Clarkson and D. G. Truhlar, *MSTor* computer program, version 2017, University of Minnesota, Minneapolis, MN, 2017.
- 115 A. D. Becke, *J. Chem. Phys.*, 1993, **98**, 5648-5652.
- 116 C. Lee, W. Yang and R. G. Parr, *Phys. Rev. B*, 1988, **37**, 785-789.
- 117 S. H. Vosko, L. Wilk and M. Nusair, *Can. J. Phys.*, 1980, **58**, 1200-1211.
- 118 E. Papajak and D. G. Truhlar, *J. Chem. Theory Comput.*, 2011, **7**, 10-18.
- 119 E. Papajak, J. J. Zheng, X. F. Xu, H. R. Leverentz and D. G. Truhlar, *J. Chem. Theory Comput.*, 2011, **7**, 3027-3034.
- 120 J.-D. Chai and M. Head-Gordon, *Phys. Chem. Chem. Phys.*, 2008, **10**, 6615-6620.
- 121 L. Goerigk and S. Grimme, *Phys. Chem. Chem. Phys.*, 2011, **13**, 6670-6688.
- 122 A. D. Laurent and D. Jacquemin, *Int. J. Quantum Chem.*, 2013, **113**, 2019-2039.
- 123 I. M. Alecu, J. J. Zheng, Y. Zhao and D. G. Truhlar, *J. Chem. Theory Comput.*, 2010, **6**, 2872-2887.
- 124 R. L. Jacobsen, R. D. Johnson, K. K. Irikura and R. N. Kacker, *J. Chem. Theory Comput.*, 2013, **9**, 951-954.
- 125 D. R. Stull, *Ind. Eng. Chem.*, 1947, **39**, 517-540.
- 126 L. Du, S. Tang, A. S. Hansen, B. N. Frandsen, Z. Maroun and H. G. Kjaergaard, *Chem. Phys. Lett.*, 2017, **667**, 146-153.
- 127 H. G. Kjaergaard, H. Yu, B. J. Schattka, B. R. Henry and A. W. Tarr, *J. Chem. Phys.*, 1990, **93**, 6239-6248.
- 128 B. I. Niefer, H. G. Kjaergaard and B. R. Henry, *J. Chem. Phys.*, 1993, **99**, 5682-5700.
- 129 M. Muro, Y. Itoh and T. Hasegawa, *J. Phys. Chem. B*, 2010, **114**, 11496-11501.
- 130 J. Simon-Kutscher, A. Gericke and H. Hühnerfuss, *Langmuir*, 1996, **12**, 1027-1034.
- 131 R. Snyder, S. Hsu and S. Krimm, *Spectrochim. Acta, Part A*, 1978, **34**, 395-406.
- 132 Q. Chen, X. Kang, R. Li, X. Du, Y. Shang, H. Liu and Y. Hu, *Langmuir*, 2012, **28**, 3429-3438.
- 133 J. Chocholoušová, J. Vacek and P. Hobza, *J. Phys. Chem. A*, 2003, **107**, 3086-3092.
- 134 C. Emmeluth, M. A. Suhm and D. Luckhaus, *J. Chem. Phys.*, 2003, **118**, 2242-2255.
- 135 R. W. Góra, M. Maj and S. J. Grabowski, *Phys. Chem. Chem. Phys.*, 2013, **15**, 2514-2522.
- 136 K. Mackeprang, Z.-H. Xu, Z. Maroun, M. Meuwly and H. G. Kjaergaard, *Phys. Chem. Chem. Phys.*, 2016, **18**, 24654-24662.
- 137 L. B. Dreier, M. Bonn and E. H. Backus, *J. Phys. Chem. B*, 2019, **123**, 1085-1089.